Superdiffusion and Viscoelastic Vortex Flows in a Two-Dimensional Complex Plasma

S. Ratynskaia,[1] K. Rypdal,[2] C. Knapek,[1] S. Khrapak,[1] A. V. Milovanov,[2] A. Ivlev,[1] J. J. Rasmussen,[3] and G. E. Morfill[1]

[1]*Max-Planck-Institut für Extraterrestrische Physik, D-85741 Garching, Germany*

[2]*Department of Physics, University of Tromso, Tromso 9037, Norway*

[3]*Risoe National Laboratory, DK-4000 Roskilde, Denmark*

(Received 29 July 2005; published 17 March 2006)

Viscoelastic vortical fluid motion in a strongly coupled particle system has been observed experimentally. Optical tracking of particle motion in a complex plasma monolayer reveals high grain mobility and large scale vortex flows coexistent with partial preservation of the global hexagonal lattice structure. The transport of particles is superdiffusive and ascribed to Lévy statistics on short time scales and to memory effects on the longer scales influenced by cooperative motion. At these longer time scales, the transport is governed by vortex flows covering a wide spectrum of temporal and spatial scales.

DOI: 10.1103/PhysRevLett.96.105010 PACS numbers: 52.27.Lw, 05.40.−a, 89.75.Da, 89.75.Fb

''Complex plasmas'' are obtained when microparticles are added to a weakly ionized gas. Under certain conditions, these charged microparticles can arrange themselves in a regular lattice structure governed by electrostatic interaction [1,2]. In certain cases, phase transition from this crystalline to a disordered state passes through the ''flow and floe'' state characterized by islands of crystalline order surrounded by streams of particles [3]. Systems studied in other experiments [4–6] exhibit ordered hexagonal structure of the entire system, and yet the grains are relatively mobile. References [4,5] reported subdiffusive transport on short time scales, due to caging of the particles, and slightly superdiffusive transport on intermediate time scales, due to the emergence and relaxation of crystal defects. In those experiments, these motions tend towards normal diffusion on even longer time scales, while superdiffusive particle transport on all time scales up to the limit given by the finite system size was reported in Ref. [6]. On the other hand, no large scale fluidlike motion has been observed in these systems. Laminar and turbulent fluid flows have been observed in several complex-plasmas experiments (e.g., [7]) but only in systems in the liquid or gaseous states.

In this Letter, we report observations of a partly ordered state in a complex plasma monolayer that allows hydrodynamic vortical flows. This state is observed in a narrow range of neutral gas pressures; the monolayer freezes at higher as well as lower pressure. The dynamics displays elastic deformation on short temporal and spatial scales but looks more like a viscous flow on larger scales; the essential characteristics of a viscoelastic flow. The basic idea of viscoelasticity can be understood in terms of the Maxwell model, where the strain γ consists of two components $\gamma = \gamma_e + \gamma_v$. The elastic component γ_e responds to the stress σ through Hooke's law $\sigma = G_0\gamma_e$ and the viscous component γ_v through the friction relation $\sigma = \eta\dot{\gamma}_v$. From these relations follows the differential equation $\sigma + \tau_M\dot{\sigma} = \eta\dot{\gamma}$, where $\tau_M = \eta/G_0$ [8]. The general solution is $\sigma(t) = (\eta/\tau_M)\int_0^\infty \dot{\gamma}\exp(-s/\tau_M)ds$, which expresses the stress as a linear response on the time history of the strain rate with an exponentially decaying response function $G(s) = (\eta/\tau_M)\exp(-s/\tau_M)$. From the differential equation, we find a viscous response $\sigma \approx \eta\dot{\gamma}$, for variations on time scales $\ll\tau_M$, and an elastic response $\sigma = G_0\gamma$, for scales $\gg\tau_M$. For oscillations at frequency ω, we have a complex Young's modulus $G^*(\omega)$, with phase angle δ given by $\tan\delta = 1/(\omega\tau)$; $\delta \ll 1$ corresponding to elastic and $\delta \approx \pi/2$ to a viscous response. The latter is used in measurements of viscoelastic responses [9]. This model implies a separation between the elastic and hydrodynamic scales given by the response time τ_M. The results presented in this Letter do not exhibit such a scale separation, as shown by the appearance of long-range memory effects in the transport of dust grains. In the present context, long-range memory means that the integral $\int_0^\infty G(s)$ diverges, as will be the case if $G(s)$ decays algebraically rather than exponentially. The origin of memory effects and elastic properties is the emergence of vortex structures on different spatial scales, inside which some stiffness (lattice order) is maintained.

The system studied is a large circular cluster of 600 dust grains in a monolayer configuration. The experiment is performed in a capacitively coupled radio-frequency discharge operated in argon at a pressure ~4 Pa and rf power of 19 W. Rough estimates of plasma parameters are $n_e \sim 10^9$ cm^{-3}, $T_e \sim 2$ eV, and $T_i \sim T_n \sim 0.03$ eV. Injected monodispersive melamine-formaldehyde spheres with diameter $2a = 7.2$ μm become negatively charged and levitate as a monolayer in the sheath above the lower electrode. The grains are confined radially by the potential created by a cavity of 6 cm radius machined into the lower electrode. The particles are illuminated by a horizontal laser sheet. 30 000 images are taken by a video camera at a sampling rate of 30 Hz and spatial resolution of 24 μm/pixel. The database consists, therefore, of 600 time series (particle coordinates) of 30 000 points each, sampled at time intervals $\delta t = 1/30$ s. The grain kinetic temperature $T_d \sim 0.15$ eV is obtained by extrapolating the grain displace-

ments at the shortest resolved time scales. Even though very weak rotation of the monolayer is detected, all data analysis has been carried out in the rotating frame of reference. The cluster diameter is 16 mm with interparticle distance $\Delta \approx 0.6$ mm. The system exhibits a hexagonal spatial structure with some five- and sevenfold defects, in particular, at the perimeter (Fig. 1). The pair correlation function (inset) reveals spatial order over distances of a few Δ. The particles are mobile, however, and on larger spatial and temporal scales vortex flows can be observed, as depicted in Fig. 2.

From the binary collision approach [10], we estimate a momentum transfer rate in dust-dust collisions $\nu_{\mathrm{dd}} \sim 17\ \mathrm{s}^{-1}$ while for dust-neutral collisions $\nu_{\mathrm{nd}} \sim 6\ \mathrm{s}^{-1}$. There is also direct evidence in the particle tracking data which supports these estimates, since we observe of the order of 100% change of particle momentum over one sampling interval $\delta t = 1/30$ s. This indicates that momentum relaxation happens on scales of the order of δt or faster. The same is confirmed by the autocorrelation function of particle velocity, which decays from unity to 0.2 within δt. Thus, there is solid evidence that there is a time scale separation for momentum relaxation in dust-dust and dust-neutral interactions, and we can consider our system as "one component," i.e., dominated by mutual interparticle collisions. We note, however, that for phenomena occurring on long time scales, where we observe large scale fluid flows, ν_{nd} introduces energy dissipation and cannot be ignored.

Essential information about the particle dynamics can be obtained by statistical analysis of the tracking data. The analysis is performed on the cumulative sum $\xi_j = \sum_{i=1}^{j} \delta\xi_i$ of the azimuthal position displacement during the sampling interval δt, defined as $\delta\xi_i = r_i \delta\varphi_i$. Here r_i is the distance from the center of the cluster at a time $i\delta t$, and $\delta\varphi_i$ is the increment in the azimuthal angle from time $(i-1)\delta t$ to $i\delta t$. The choice of the quantity ξ_j is motivated by the fact that it is not limited by the boundary in contrast to the radial position r_j. The *variogram* of the process ξ_j is defined as $V(\tau) = (N - \tau/\delta t)^{-1} \sum_{j=1}^{N-\tau/\delta t} (\xi_{j+\tau/\delta t} - \xi_j)^2$; i.e., it is the variance of the probability distribution function (PDF) of azimuthal position increments $\Delta\xi_j(\tau) = \xi_{j+\tau/\delta t} - \xi_j$ over the time lag τ. An example of such a PDF for $\tau \sim 2$ s is shown in Fig. 3(a). The standard deviation $\sigma(\tau) \sim \sqrt{V(\tau)}$ grows with time as a power law $\sigma(\tau) \sim \tau^H$ and is plotted in Fig. 3(b). The Hurst exponent H lies in the range between 0 and 1. Our results indicate that $H \approx 0.84$ for $\tau \lesssim 10$ s and $H \approx 0.68$ for $\tau \gtrsim 10$ s. This second value persists up to the longest time scales accessible in our study, $\tau \sim 500$ s. The fact that H is larger than 0.5 implies that the transport is superdiffusive. For times τ shorter than $\sim$30 s, the PDF of azimuthal displacements is consistent with a stretched Gaussian distribution

$$P(\Delta\xi, \tau) = A(\tau) \exp[-B(\tau)|\Delta\xi|^{2\mu}] \qquad (1)$$

and time-varying coefficients $A(\tau)$ and $B(\tau)$. Figures 3(c) and 3(d) show that these are best fitted to inverse power law dependencies $A(\tau) \sim \tau^{-\zeta/\mu}$ and $B(\tau) \sim \tau^{-2\zeta}$ in two separate regimes for τ. From the PDF in Eq. (1), one finds the

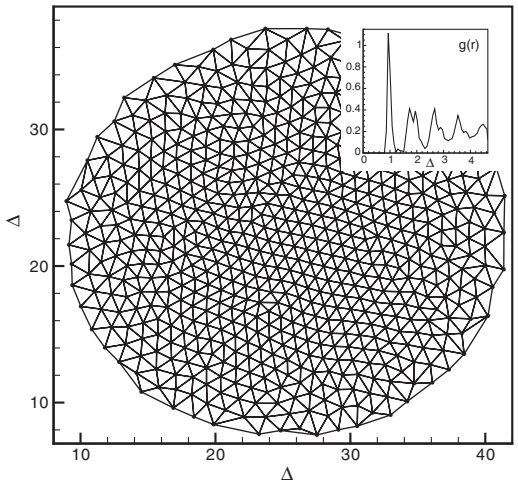

FIG. 1. A snapshot of the particle system showing strongly ordered structure and the pair correlation function (inset).

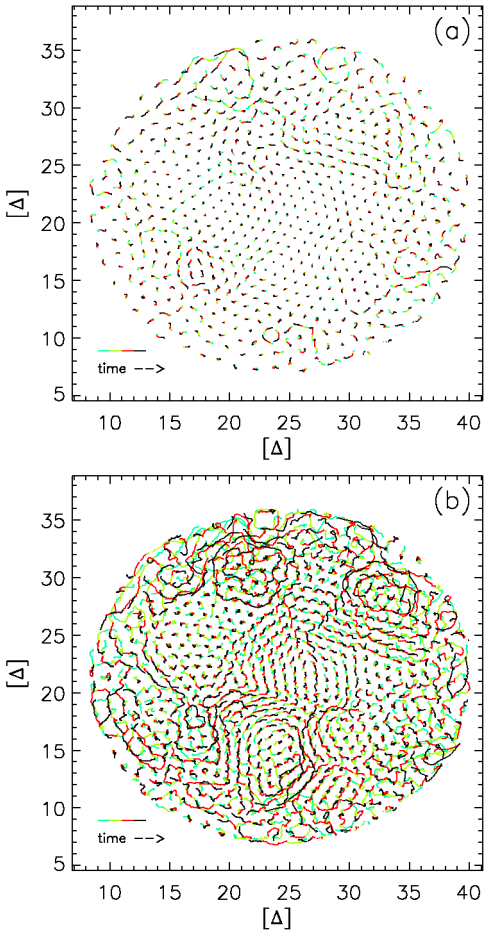

FIG. 2 (color online). Motion of particles during (a) $\sim$1 s and (b) $\sim$10 s.

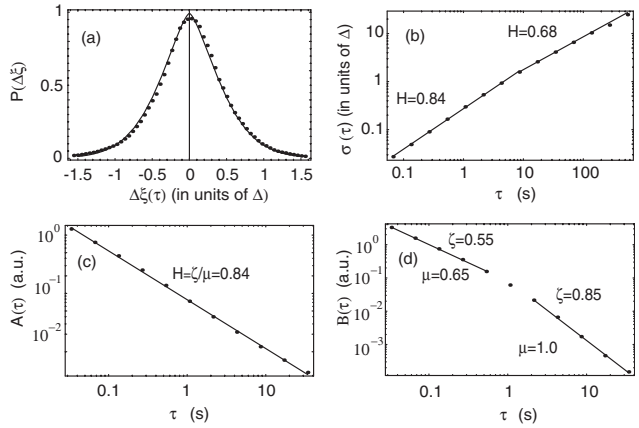

FIG. 3. (a) PDF of azimuthal position increments for time lag $\tau = 2$ s (dots). The nonlinear fit is the function given by Eq. (1) (solid curve). (b) Plot of $\sigma(\tau)$ [see text for definition]. (c),(d) Plot of $A(\tau)$ and $B(\tau)$ [see Eq. (1) for definition].

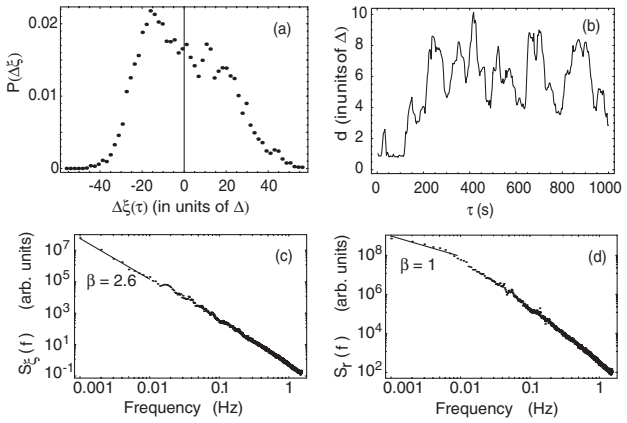

FIG. 4. (a) PDF of azimuthal position increments for time lag $\tau = 500$ s. (b) An example of relative diffusion (distance d between two particles as a function of time). (c),(d) Power spectra of azimuthal $[S_\xi(f) \sim f^{-\beta}]$ and radial $[S_r(f) \sim f^{-\beta}]$ displacements, with $\beta \sim 2.6$ and $\beta \sim 1$ for $f < 0.01$ Hz, respectively.

standard deviation $\sigma(\tau) \sim \tau^{\zeta/\mu}$, leading to $H = \zeta/\mu$. From Fig. 3(c), we find that $\zeta/\mu \approx 0.84$ for $\tau \lesssim 10$ s, consistent with the value found for H from the variogram analysis shown in Fig. 3(b). However, by plotting the coefficient $B(\tau)$ as in Fig. 3(d), we find that the exponents μ and ζ depend on τ, even though their ratio $H = \zeta/\mu \approx 0.84$ is almost constant up to $\tau \sim 10$ s. In fact, for the short times $\tau \lesssim 1$ s, we have $\zeta \approx 0.55$ and $\mu \approx 0.65$. These change to $\zeta \approx 0.84$ and $\mu \to 1$ for $\tau \gtrsim 1$ s. The fact that $\mu \to 1$ simply means that Eq. (1) tends to a Gaussian distribution on time scales $\tau > 1$ s. Since the Hurst exponent $H \approx 0.84$ is still larger than 0.5, the process is compatible with a persistent fractional Brownian motion (FBM), a self-affine, Gaussian stochastic process which exhibits long-range memory [11]. An ordinary Brownian motion appears as a summation of a Gaussian white noise process and an FBM as a summation of white noise filtered in favor of the low frequencies. The physics of this filtering is the emergence of cooperative hopping and vortex motions on time scales on which particles can move a distance Δ or more.

The more heavy-tailed PDF observed on shorter time scales indicates that the enhanced diffusion for $\tau \lesssim 1$ may be governed by mechanisms other than memory. Superdiffusion in the absence of long-range memory is normally ascribed to Lévy processes [12], for which the PDFs exhibit algebraic tails $P(\Delta\xi) \sim |\Delta\xi|^{-\mu}$. Algebraic tails are not observed here, but it is conceivable that the longer "Lévy flights" are prevented by some dissipative mechanism, e.g., neutral drag. This mechanism would then effectively truncate the tail of the PDF. The core of the Lévy PDF can be shown to converge to the stretched Gaussian distribution in Eq. (1) [13].

After approximately 30 s, the nearly Gaussian PDF develops an asymmetry, and at $\tau \approx 500$ s it has split up into two large and some smaller humps, as seen from Fig. 4(a). These humps show that the superdiffusive transport observed on time scales up to 30 s is replaced by advection of subpopulations of particles trapped in vortices of varying size. For the results $P(\Delta\xi, \tau)$ presented in Figs. 3, 4(a), 4(c), and 4(d), the study was based on a sample of 200 particles initially grouped together in one region of the cluster. The majority of these particles belong to the "interior," so on short time scale $\tau < 30$ s the statistics reflects typical interior behavior. In an edge boundary layer a few interparticle distances wide, the crystal bonds are weaker and the grains move more or less like in the liquid state. This fluid motion in the edge contributes to the long-time statistics presented in Fig. 4, but plots of individual trajectories show that the main transport of grains occurs in the interior, so the flow picture emerging from the statistical analysis on long time scales is also characteristic for the dynamics in the interior of the cluster.

Additional support for the vortex flow interpretation can be found from the relative diffusion of the particles. Figure 4(b) shows the evolution of the distance d between two particles that start out as nearest neighbors ($d \approx \Delta$ at $t = 0$). On time scales of the order of some tens of seconds, one observes jumps in d of approximately one Δ, sometimes as single slip events but more often as a continuous chain of several consecutive slips. On longer time scales, these cooperative events form oscillatory motions over a broad spectrum of frequencies corresponding to trapping of the two particles in vortices of varying size up to the size of the system. The same can be deduced from the power spectrum of azimuthal displacements $S_\xi(f) \sim f^{-\beta}$, with $\beta \sim 2.6$ for frequencies below 0.1 Hz [Fig. 4(c)]. The relation to the Hurst exponent is $H = (\beta - 1)/2$, giving $H \approx 0.8$ for $\tau > 10$ s, somewhat higher than found from the variogram in Fig. 3(b). The latter estimate is more reliable, since it is known that the variogram underestimates the true self-affinity parameter for strongly super-

diffusive fractional Brownian motions [11]. The power spectrum of radial displacements $S_r(f) \sim f^{-\beta}$ has $\beta \sim 1$ for the frequency range lower than 0.01 kHz [Fig. 4(d)]. The corresponding variogram (not shown) departs from the variogram for the azimuthal displacement for $\tau > 10$ s and becomes flat for $\tau > 100$ s. This is due to the limitation of the radial displacement set by the finite cluster size. The spectral index $\beta = 1$ ($H_a = 0$) on the hydrodynamic time scale $\tau > 100$ s corresponds to an antipersistent process at the transition between a ''noise'' process (stationary) and a ''motion'' (nonstationary), also called ''pink noise'' or ''$1/f$ noise'' [11].

The idea that the grain dynamics can be described as a viscoelastic flow derives mainly from figures of the flow patterns such as Fig. 2 (and study of the movies [14]) and from the results of the statistical studies presented in Figs. 3 and 4. In Fig. 2, one observes large domains where motion on time scales <30 s occurs along the three principal directions (crystal surfaces) in a hexagonal crystal structure, and yet the collective motion has the character of rotation of this domain (a vortex). The edges of the domains follow the crystal surfaces, and in their interior the crystal order is maintained; i.e., on this time scale, grains do not interchange positions in the lattice. Geometric constraints then imply a certain deformation (strain) of the domain as it rotates, and the resulting stress corresponds to elastic behavior. On the border between domains, development of crystal defects allows grains to slip relative to each other, and on these boundaries the stress depends on the strain *rate* rather than the strain itself; i.e., the motion is viscous. If there were one characteristic vortex size and turnover time, we would have two distinct scales: elastic on small scales and viscous on large. However, since Fig. 2, as well as Figs. 4(a) and 4(b) indicate a wide range of vortex sizes, it is not possible to separate these scales, and the statistically averaged stress-strain relation may exhibit a ''long-range'' response function $G(s) \sim s^{-\alpha}$, with $\alpha \leq 1$. On time scales below a few dust-neutral relaxation times ν_{dn}^{-1}, the transport seems to be governed by Lévy statistics where the algebraic tails of the distribution are truncated, possibly due to the effects of collisions with neutrals. On longer time scales, the transport is superdiffusive due to memory effects. Long-range memory means that the long scales are more strongly represented in the spectrum, indicating that vortex motions on varying scales are responsible for this memory-based superdiffusion.

For a complete description of the system, we also need to understand the mechanisms responsible for energization of the dust grains and driving the vortical flow against the neutral gas friction. As has been pointed out by Zhakhovskii *et al.* [15], the fact that the particle charge depends on the spatial coordinates implies that the energy of particles in external electric fields is not conserved. This is because the external electrostatic force is no longer potential. The sign of the work done on a particle over a closed path depends on the direction of motion along the path; hence, the formation of vortical patterns is consistent with a balance between positive energy gain over the cycle and the frictional loss due to neutral drag, as recently suggested in Refs. [16,17]. Therefore, one of the possible driving mechanisms of the observed vortex formation can be the charge inhomogeneity across the layer. Another energy source for horizontal particle motion (especially at the short time scales) might arise from the interaction with the wakes which are formed under each particle by the downward streaming ions (see, e.g., [18]). It has been shown that the wakes can cause horizontal acceleration of a single particle suspended *under* the main layer [19], and one cannot exclude the possibility that a similar mechanism affects particles in the layer.

[1] J. H. Chu and Lin I, Phys. Rev. Lett. **72**, 4009 (1994).
[2] H. Thomas, G. E. Morfill, V. Demmel, J. Goree, B. Feuerbacher, and D. Mohmann, Phys. Rev. Lett. **73**, 652 (1994).
[3] H. Thomas and G. E. Morfill, Nature (London) **379**, 806 (1996).
[4] Ying-Ju Lai, Wei-Yen Woo, and Lin I, Plasma Phys. Controlled Fusion **46**, B449 (2004).
[5] Chia-Ling Chan *et al.*, Plasma Phys. Controlled Fusion **47**, A273 (2005).
[6] S. Ratynskaia *et al.*, Phys. Plasmas **12**, 022302 (2005).
[7] G. E. Morfill *et al.*, Phys. Rev. Lett. **92**, 175004 (2004).
[8] L. D. Landau and E. M. Lifschitz, *Theory of Elasticity* (Pergamon, Oxford, 1986), 3rd ed.
[9] R. S. Lakes, Rev. Sci. Instrum. **75**, 797 (2004).
[10] S. A. Khrapak, A. V. Ivlev, and G. E. Morfill, Phys. Rev. E **70**, 056405 (2004).
[11] S. Hergarten, *Self-Organized Criticality in Earth Systems* (Springer, Berlin, 2002).
[12] P. Wolfgang and J. Baschnagel, *Stochastic Processes, From Physics to Finance* (Springer, Berlin, 1999).
[13] A. V. Milovanov (unpublished).
[14] Grain trajectories during 30 s can be viewed at http://www.mpe.mpg.de/complex-plasmas/visco-elastic/figure.ps.
[15] V. V. Zhakhovskii *et al.*, JETP Lett. **66**, 419 (1997).
[16] O. S. Vaulina *et al.*, Plasma Phys. Rep. **30**, 918 (2004).
[17] S. K. Zhdanov, A. V. Ivlev, and G. E. Morfill, Phys. Plasmas **12**, 072312 (2005).
[18] A. Melzer, V. A. Schweigert, and A. Piel, Phys. Rev. Lett. **83**, 3194 (1999).
[19] V. A. Schweigert *et al.*, Phys. Plasmas **9**, 4465 (2002).